*Human Molecular Genetics*, 2017, Vol. 26, No. 23 4699–4714

**doi: 10.1093/hmg/ddx352**
Advance Access Publication Date: 11 September 2017
Original Article

ORIGINAL ARTICLE

# A novel *SYN1* missense mutation in non-syndromic X-linked intellectual disability affects synaptic vesicle life cycle, clustering and mobility

Fabrizia C. Guarnieri[1,2], Davide Pozzi[3], Andrea Raimondi[4], Riccardo Fesce[5], Maria M. Valente[1], Vincenza S. Delvecchio[1], Hilde Van Esch[6], Michela Matteoli[3,7], Fabio Benfenati[8,9], Patrizia D'Adamo[1] and Flavia Valtorta[1,2,*]

[1]Division of Neuroscience, San Raffaele Scientific Institute, 20132 Milan, Italy, [2]San Raffaele Vita-Salute University, 20132 Milan, Italy, [3]Laboratory of Pharmacology and Brain Pathology, Humanitas Clinical and Research Center, 20089 Rozzano, Milan, Italy, [4]Experimental Imaging Center, San Raffaele Scientific Institute, 20132 Milan, Italy, [5]Centre of Neuroscience and DISTA, University of Insubria, 21100 Varese, Italy, [6]Center for Human Genetics, University Hospitals Leuven, B3000 Leuven, Belgium, [7]CNR Institute of Neuroscience, Milan, Italy, [8]Department of Experimental Medicine, University of Genova, 16132 Genova, Italy and [9]Center for Synaptic Neuroscience and Technology, Istituto Italiano di Tecnologia, 16132 Genova, Italy

*To whom correspondence should be addressed at: DIBIT 3A2, San Raffaele Scientific Institute, Via Olgettina 58, 20132 Milan, Italy. Tel: +390226434826; Fax: +390226434844; Email: valtorta.flavia@hsr.it

## Abstract

Intellectual Disability is a common and heterogeneous disorder characterized by limitations in intellectual functioning and adaptive behaviour, whose molecular mechanisms remain largely unknown. Among the numerous genes found to be involved in the pathogenesis of intellectual disability, 10% are located on the X-chromosome. We identified a missense mutation (c.236 C > G; p.S79W) in the *SYN1* gene coding for synapsin I in the MRX50 family, affected by non-syndromic X-linked intellectual disability. Synapsin I is a neuronal phosphoprotein involved in the regulation of neurotransmitter release and neuronal development. Several mutations in *SYN1* have been identified in patients affected by epilepsy and/or autism. The S79W mutation segregates with the disease in the MRX50 family and all affected members display intellectual disability as sole clinical manifestation. At the protein level, the S79W Synapsin I mutation is located in the region of the B-domain involved in recognition of highly curved membranes. Expression of human S79W Synapsin I in *Syn1* knockout hippocampal neurons causes aberrant accumulation of small clear vesicles in the soma, increased clustering of synaptic vesicles at presynaptic terminals and increased frequency of excitatory spontaneous release events. In addition, the presence of S79W Synapsin I strongly reduces the mobility of synaptic vesicles, with possible implications for the regulation of neurotransmitter release and synaptic plasticity. These results implicate *SYN1* in the pathogenesis of non-syndromic intellectual disability, showing that alterations of synaptic vesicle trafficking are one possible cause of this disease, and suggest that distinct mutations in *SYN1* may lead to distinct brain pathologies.

**Received:** July 27, 2017. **Revised:** August 25, 2017. **Accepted:** August 29, 2017

## Introduction

The term Intellectual Disability (ID) refers to a heterogeneous group of disorders with onset during the developmental period and characterized by deficits in intellectual functions and adaptive behaviours that impact on the conceptual, social and practical domains of the person (1). Syndromic and non-syndromic ID can be distinguished, depending on whether patients display multi-organ involvement or intellectual impairment is the only clinical manifestation, respectively. The prevalence estimates of ID are highly variable, due to the huge phenotypic heterogeneity and difficulties in patient stratification, but many studies agree on a value of approximately 1% in the overall population (2). Comorbidity with other cognitive disorders is often observed, particularly with autism spectrum disorder (ASD), as it is estimated that 40% of ID patients are also affected by ASD and, conversely, that 50-85% of ASD patients show ID (3,4).

Genetic causes probably account for the majority of moderate-to-severe ID cases; still, many patients lack a molecular diagnosis. Genetic defects include large chromosomal aberrations, submicroscopic deletions/duplications, as well as monogenic defects and single-nucleotide variations (5,6). The identification of individual genes involved in ID is continuously evolving. The exact number of ID genes varies according to the developmental disorders that are taken into consideration, but recent reports list >800 protein-coding genes involved in syndromic and non-syndromic ID, of which more than 10% are X-linked (7). Many of these genes converge on few common functional networks, as many ID proteins participate in the same cellular and molecular processes, including neurogenesis, neuronal migration, synapse formation and functioning (8). Several ID causative mutations have been found in genes coding for proteins involved in synaptic vesicle (SV) recycling at the presynaptic terminal, such as αGDI (Rab GDP-dissociation inhibitor alpha), RAB3GAP (Rab3 GTPase-activating protein) or MUNC-18 (9–13).

Nonsense and missense mutations in the *SYN1* and *SYN2* genes, encoding the presynaptic proteins Synapsin (Syn) I and II, have been identified in patients affected by epilepsy in combination with learning disability (14) or ASD (15,16). Synapsins are a family of three neuronal proteins (SynI, SynII and SynIII), which display redundant, as well as distinct, structural and functional features (17). The most characterized member is SynI, a protein that reversibly associates with the surface of SVs and the actin cytoskeleton in a phosphorylation-dependent manner. By virtue of these properties and of its ability to oligomerize, SynI mediates the clustering of SVs in the presynaptic terminal, regulates the number of SVs available for exocytosis and facilitates the postdocking steps of exocytosis (17). Through this mechanism, SynI directly modulates neurotransmitter release and finely tunes synaptic strength and plasticity (18). In addition, SynI plays a role in synaptogenesis and neurite outgrowth during neuronal development (19).

We have identified a novel missense mutation in the *SYN1* gene (c.236 C > G, S79W) in the MRX50 family, a European family affected by non-syndromic X-linked ID (XLID) with no clinical history of epilepsy or ASD (20). The mutation causes the substitution of a phylogenetically conserved Serine residue with a Tryptophan, with possible severe implications for the folding and function of the protein. We characterized the effects of S79W SynI expression in heterologous HeLa cells and in *Syn1* knock-out (KO) hippocampal neurons in culture. We found that S79W SynI promotes the formation of aberrant perinuclear accumulations of small clear vesicles. In addition, in neurons it affects SV clustering at presynaptic terminals, spontaneous SV release and SV mobility. These data support a causative role of this mutation and the derived functional alterations of synaptic function in determining the ID phenotype in the MRX50 family.

## Results

### Identification of the c.236 C > G (p.S79W) mutation in the MRX50 family

Several *SYN1* mutations have been described in families affected by epilepsy and/or ASD, in some cases associated with cognitive disability (14,15). We therefore investigated whether mutations in this gene, located on the X chromosome, might be associated with a primary cognitive phenotype and XLID. In collaboration with the EuroMRX Consortium (http://euromrx.com; date last accessed September 15, 2017), we selected 12 families mapped by linkage analysis to the *SYN1* locus, Xp11.23 (Supplementary Material, Table S1) (21). These 12 families were screened for the presence of mutations in the *SYN1* gene by direct sequencing of the entire coding region (13 exons including splicing sites), 5'/3' untranslated regions (UTR) and part of the proximal promoter region in one proband/family. The sequence obtained was compared with the reference human genomic sequence available in the NCBI (accession number: NG_008437.1) and Ensembl (accession number: ENSG00000008056) databases. The screening resulted in the identification of a point mutation in the coding region of the gene in one of the probands analysed, belonging to the L027 family (see Supplementary Material, Table S1). This family, also annotated as MRX50, displayed a lod score >2 with the *SYN1* locus in the linkage analysis. The mutation consisted in a C-to-G transition in the 1$^{st}$ exon of the *SYN1* gene (c.236 C > G) (Fig. 1A). The presence of the c.236 C > G mutation was assessed in the rest of the MRX50 family. All affected males whose DNA was available carried the mutation, which was absent in healthy members and present in heterozygous state in an obligate carrier female. In addition, the mutation was absent in 151 healthy control males analysed, as well as in dbSNP (http://www.ncbi.nlm.nih.gov/projects/SNP/; date last accessed September 15, 2017), in the Exome Variant Server (6503 individuals, NHLBI GO Exome Sequencing Project (ESP), Seattle, WA; http://evs.gs.washington.edu/EVS/), in the ExAC Browser (http://exac.broadinstitute.org/; date last accessed September 15, 2017) and in the 1000 Genome Project (2504 individuals, http://www.1000genomes.org/; date last accessed September 15, 2017) (22). The complete pedigree of the family, clearly indicating a X-linked mode of inheritance, is shown in Figure 1B. The clinical characterization of the MRX50 patients has been previously published (20). Patients were described as affected by a moderate to severe ID, appearing at approximately 6 years of age and requiring special education. The obligate carrier female IV-11 had a reduced intelligence. Patients showed no other phenotypic abnormalities and their neurological profile was normal, with no epileptic seizures reported. The pathological phenotype was therefore classifiable as a non-syndromic form of XLID. This was also confirmed by our evaluation of the only surviving patient of the family (V-19), performed in 2011. This man was 81 years old and lived in a nursing home. He had a moderate ID, severe perseveration and echolalia, but no other stereotypies, dysmorphisms or phenotypic abnormalities (normal testis volume and head size). From the medical files of the family, neither the patient nor any of the affected males was ever reported to have experienced seizures. The patient died in 2012, and no new affected males were born because most females were appropriately counselled.

At the protein level, the nucleotide transition identified results in the substitution of Serine 79 (Ser/S, codified by a TCG

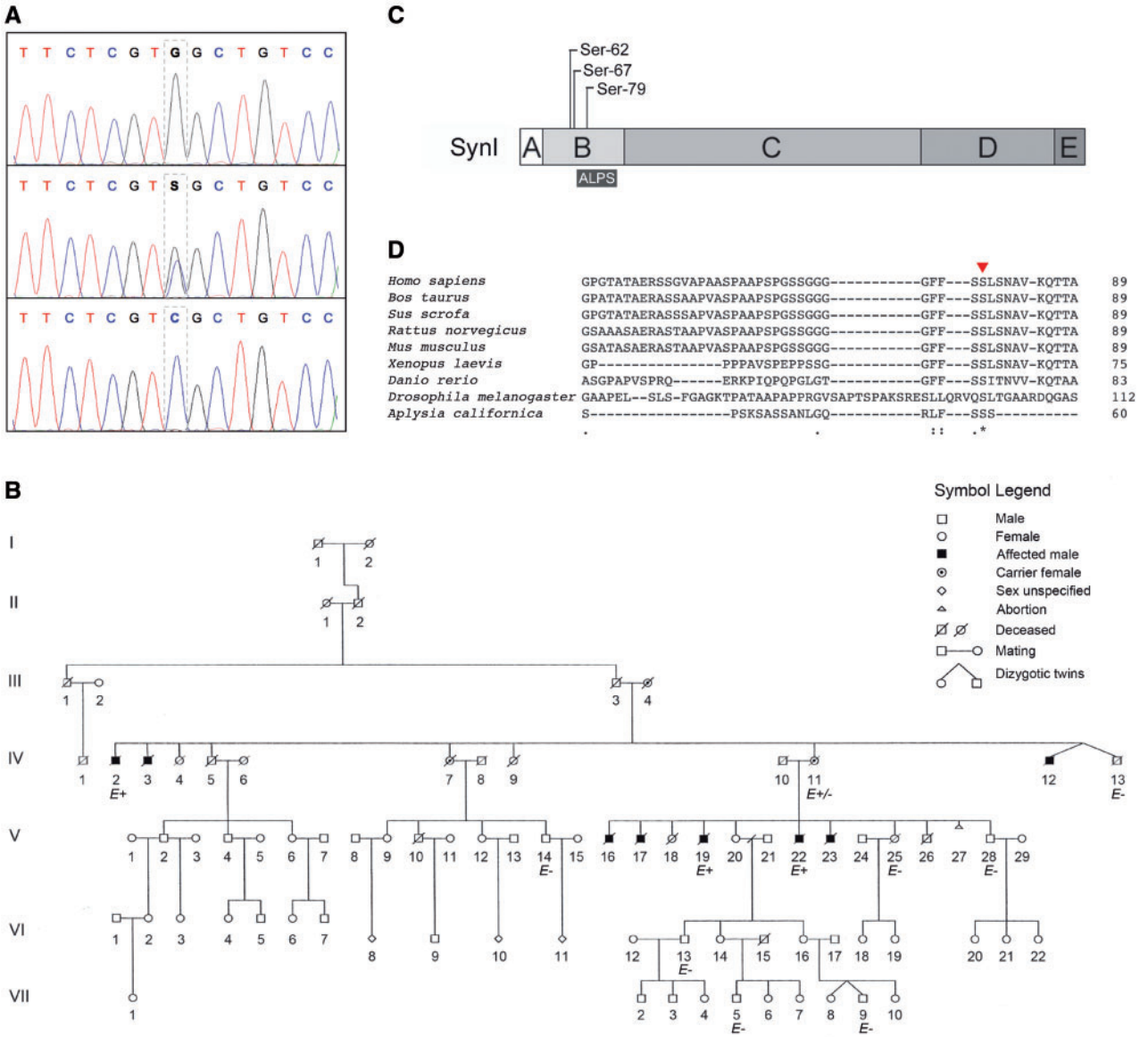


**Figure 1.** Identification of the c.236 C > G/S79W mutation in the MRX50 family. (**A**) Representative electropherograms of *SYN1* genomic sequences of an affected male (*upper panel*), an obligate carrier female (*middle panel*) and a healthy subject (*bottompanel*). (**B**) Pedigree of the MRX50 family, showing an X-linked mode of inheritance. Genomic DNA was available and analysed for members indicated with *E* (*E*+: mutation carrier; *E*-: non carrier). The index was V-19. Female IV-11 is an obligate carrier (*E*+/-), as she had both affected and unaffected sons. (**C**) Schematic representation of the SynI domain model. Ser-79 is replaced by Tryptophan in the MRX50 patients. Ser-79 lies in close proximity to the MAPK phosphorylation sites 4 and 5 (Ser-62 and Ser-67) and within the ALPS (amphipathic lipid packing sensor) motif. (**D**) Alignment of the SynI protein sequence across species. Numbers on the right indicate the last amino acid position of the line. The degree of conservation is indicated at the bottom, with 'asterisk' being residue identity in all species, 'colon' conservation between strongly similar groups of amino acids, and 'dot' conservation between weakly similar residues. Ser-79 is indicated with a red arrowhead.

codon) with a Tryptophan (Trp/W, TGG codon). Ser-79 lies in domain B of SynI (Fig. 1C). This domain contains a membrane curvature sensor motif named amphipathic lipid packing sensor (ALPS), which facilitates SynI association with SVs (23). The S79W substitution may strongly impact on the folding of the motif. Indeed, the bioinformatics tool PolyPhen-2 (24) predicted a high probability of damage for the S79W substitution on SynI protein structure, giving maximal scores (0.998-1) with two different false positive rate thresholds. In addition, Ser-79 lies in very close proximity to two important phosphorylation sites (Ser-62 and Ser-67), which are targeted by mitogen-activated protein kinase (MAPK) and modulate SynI binding to SVs and actin (25,26), and to an O-glycosylation site (Thr-87) that regulates SynI localization to synapses (27). Thus, the S79W substitution might also affect the accessibility of these residues to MAPK and N-acetylglucosamine transferase, and derange SynI post-translational modifications.

The phylogenetic alignment of the SynI protein sequence showed that Ser-79 is highly conserved among species from *Aplysia* to human (Fig. 1D), raising the possibility that this site is evolutionarily important for SynI function. This residue has never been described as being post-translationally modified. The bioinformatics tools NetOGlyc 4.0 (28) and NetPhos 3.1 (29) did not predict Ser-79 as a possible target of O-glycosylation or phosphorylation, aside from a barely significant prediction as substrate for cyclin-dependent kinase 1 (Cdk1).

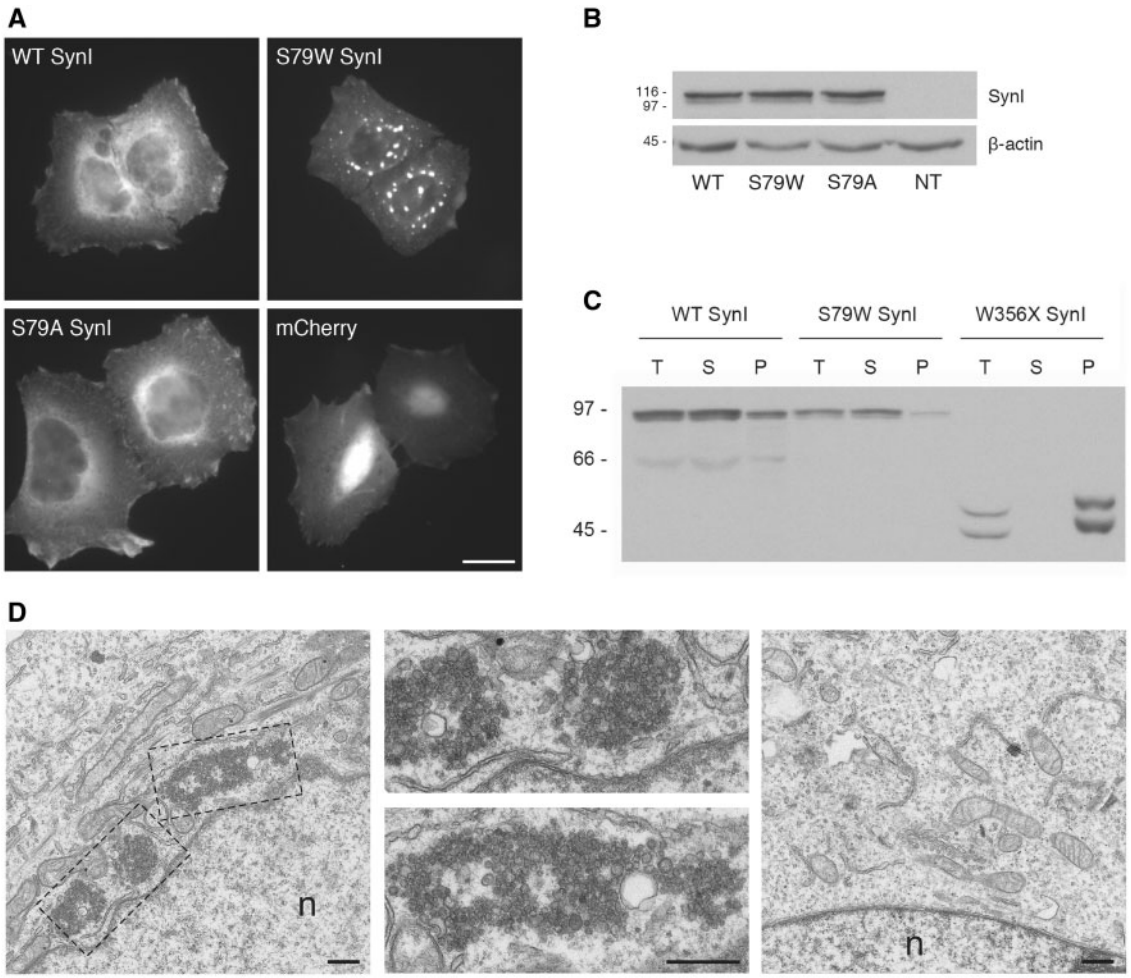


**Figure 2.** S79W SynI expression in HeLa cells leads to the formation of soluble aggregates composed of small clear vesicles. (**A**) Representative fluorescence images of HeLa cells transfected with plasmids coding for mCherry-tagged WT or mutant SynI, or for the mCherry tag alone. Scale bar: 15 μm. (**B**) Representative Western Blot of HeLa cells transfected with mCherry-tagged constructs and lysed in RIPA buffer. β-actin was used as loading control. NT: non-transfected control. (**C**) Representative Western Blot showing detergent solubility of S79W aggregates. HeLa cells were transfected with FLAG-tagged WT, S79W or W356X Syn I constructs. Protein solubility was assessed through cell lysis with 1% Triton X-100. The lysates were separated into pellet and supernatant fractions, and equal volumes of total lysate (T), pellet (P), or supernatant (S) fractions were analysed by immunoblotting with an anti-SynI antibody (G143). (**D**) Transmission electron microscopy images of HeLa cells transfected with mCherry-tagged S79W (*left panel*) or WT (*right panel*) SynI. The middle panels show higher magnifications of the areas highlighted in the *left* panel. n: nucleus. Scale bars: 500 nm.

## S79W SynI promotes the formation of perinuclear accumulations of small clear vesicles in HeLa cells and hippocampal neurons

In order to study the effects of the S79W mutation on SynI structure and function, we produced plasmid constructs encoding either the WT or the S79W human SynI protein fused with the red fluorescent protein mCherry. When transfected in HeLa cells grown in culture, the S79W mutant protein formed large perinuclear aggregates that were never observed in WT SynI-transfected cells. Interestingly, the expression of a pseudo-control SynI mutant bearing a more conservative residue substitution (Ser-to-Ala, S79A) did not induce the formation of aggregates and the protein appeared diffused in the cell cytoplasm like the WT SynI (Fig. 2A). To exclude that this effect was due to the fluorescent tag used, we produced FLAG-tagged and untagged WT and mutant human SynI, as well as untagged WT and mutant murine SynI plasmidic constructs. In all cases, the aggregation phenotype was observed only with the S79W SynI variant (Supplementary Material, Fig. S1). Thus, we decided to use the mCherry-tagged constructs for all subsequent experiments.

The expression levels of S79W SynI, as assessed through Western blotting in HeLa cells (Fig. 2B), were identical to those of the WT and S79A isoforms, suggesting that the mutation does not affect protein synthesis or stability. Aggregate solubility in Triton-X100 was tested through Western blot analysis of total lysates, supernatants and Triton-insoluble pellets from transfected HeLa cells. WT and S79W SynI were largely extracted in the Triton-soluble fraction (Fig. 2C). On the contrary, the aggregates formed by the W356X SynI variant —the first *SYN1* mutation identified in epileptic patients (14)—were virtually insoluble, as previously reported (30).

At the ultrastructural level, HeLa cells expressing S79W SynI were characterized by the presence of large clusters of small clear vesicles, which were never observed in cells transfected with the WT SynI isoform (Fig. 2D). Interestingly, when HeLa cells were co-transfected with a construct coding for the transmembrane SV protein synaptophysin tagged with the enhanced

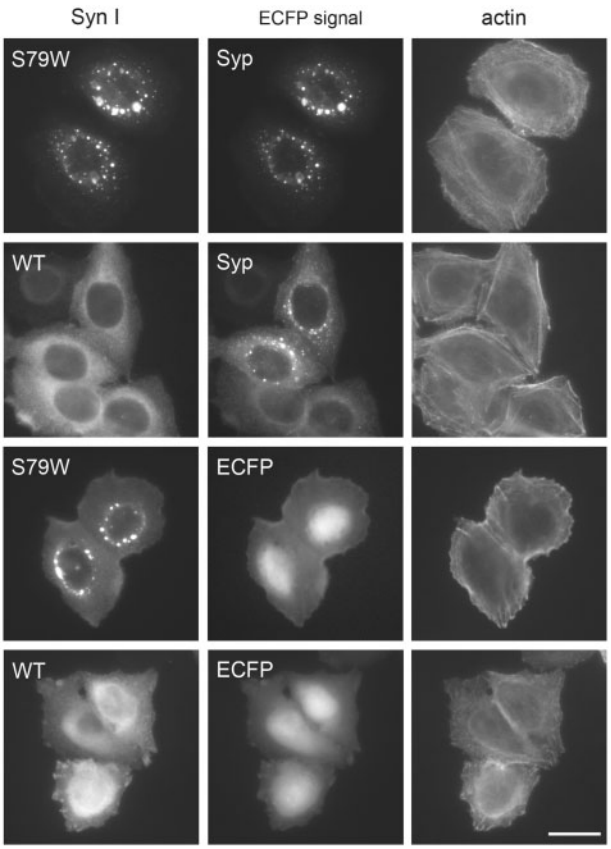


**Figure 3.** The synaptic vesicle protein synaptophysin-ECFP is sorted to S79W SynI aggregates. HeLa cells were co-transfected with WT or S79W mCherry-tagged SynI and either Synaptophysin-enhanced cyan fluorescent protein (Syp-ECFP) or ECFP. Phalloidin staining marks the actin cytoskeleton for recognition of cell morphology. Scale bar: 15 μm.

cyan fluorescent protein (Syp-ECFP), Syp was completely sequestered in S79W SynI aggregates (Fig. 3). Conversely, in cells transfected with WT SynI, Syp-ECFP showed a punctate staining that only rarely co-localized with SynI. S79W SynI might therefore be able to promote the accumulation of vesicular organelles intrinsically competent for sorting SV proteins in heterologous cells that do not endogenously express them.

Next, we tested the expression of S79W SynI in primary neuronal cells. High efficiency of transduction was achieved through lentiviral infection. In order to recapitulate the neurobiological conditions of the MRX50 patients and avoid possible artefacts caused by SynI overexpression, all experiments in primary neuronal cells were performed using *Syn1* KO neurons in which we reintroduced either WT or S79W SynI. Hippocampal neurons were infected at 10 DIV, and analysed at 17 DIV. The expression levels of WT and S79W SynI were comparable, as assessed through Western blotting (Fig. 4A). In analogy with what observed in HeLa cells, also in neurons the S79W SynI protein formed large somatic accumulations that co-localized with the SV marker vesicular glutamate transporter 1 (VGLUT1) and that were absent in cells transduced with WT SynI (Fig. 4B). Electron microscopy analysis showed that the expression of S79W SynI was able to cause the accumulation, in the neuronal somata, of small clear vesicles with homogeneous diameter (40–60 nm, consistent with SV dimension) (Fig. 4Ca). Such abnormal clusters of vesicles were also observed in other cellular districts, as they appeared to be aberrantly transported in dendrites (Fig. 4Cb). This kind of structures was never visible in neurons transduced with WT SynI (Fig. 4Cc). Interestingly, in both HeLa cells and neurons, the somatic accumulations of small clear vesicles were often in close apposition to the Golgi cisternae, raising the possibility that S79W SynI is able to promote an aberrant production of vesicles (possibly, SV precursor vesicles in neurons) through the budding from Golgi membranes (Supplementary Material, Fig. S2). S79W SynI was not completely sequestered in perinuclear accumulations, but was still able to reach *bona fide* presynaptic terminals, as the number of puncta positive for the presynaptic protein Bassoon and for SynI was comparable in neurons expressing either S79W or WT SynI (Fig. 4D).

## S79W SynI expression does not affect early neuronal development

Syns have been shown to have a role in the first stages of neuronal development (31). We tested the effects of S79W SynI expression on neurite elongation and axonal branching in cultured *Syn1* KO hippocampal neurons. To this aim, neurons were electroporated at 0 DIV with plasmidic constructs coding for either mCherry-tagged WT SynI, S79W SynI or mCherry alone. Cells were fixed at 1.5 DIV and stained for βIII-tubulin, which decorates the entire neuronal profile. The number and length of neurites of mCherry-positive isolated cells were measured for each condition. The analysis failed to reveal defects in total neurite length, axonal length or number of axonal branches in neurons expressing S79W SynI compared with neurons expressing either WT SynI or mCherry (Fig. 5A–D).

## S79W SynI expression increases the frequency of miniature excitatory postsynaptic currents and the number of synaptic vesicles at presynaptic terminals

Given the well-established role of SynI in the regulation of neurotransmitter release at mature presynaptic terminals, we evaluated the effects of S79W SynI on basal synaptic transmission in mature neurons. Patch-clamp recordings of miniature excitatory and inhibitory postsynaptic currents (mEPSCs and mIPSCs) were performed in *Syn1* KO hippocampal neurons transduced with lentiviruses coding for either mCherry-tagged WT SynI, S79W SynI or mCherry alone. Neurons were infected at 10 DIV and analysed at 16-17 DIV. The expression of S79W SynI caused a significant increase in the frequency of mEPSCs as compared with neurons expressing either WT SynI or mCherry alone (Fig. 6A and B). The amplitude of mEPSCs was unaffected in all cases (Fig. 6C). The input resistance (mCherry: 149.85 ± 8.99 mΩ; WT SynI: 139.15 ± 8.85 mΩ; S79W SynI: 126.19 ± 5.65 mΩ mean ± SEM) and resting potential (mCherry: -59.37 ± 1.04 mV; WT SynI: -61.16 ± 1.18 mV; S79W SynI: -60.6 ± 0.90 mV mean ± SEM) were not statistically different under the three conditions analysed, indicating that the passive properties of the cells were not altered by the expression of S79W SynI. Concerning GABAegic transmission, mIPSC frequency and amplitude were not significantly different in neurons expressing either mCherry-tagged WT SynI, S79W SynI or mCherry alone (Fig. 6D–F). These results indicate that the expression of S79W SynI leads to a marked presynaptic effect selectively in excitatory neurons.

In order to understand the cellular bases for the increased mEPSC frequency in S79W SynI expressing neurons, we performed transmission electron microscopy analyses. In

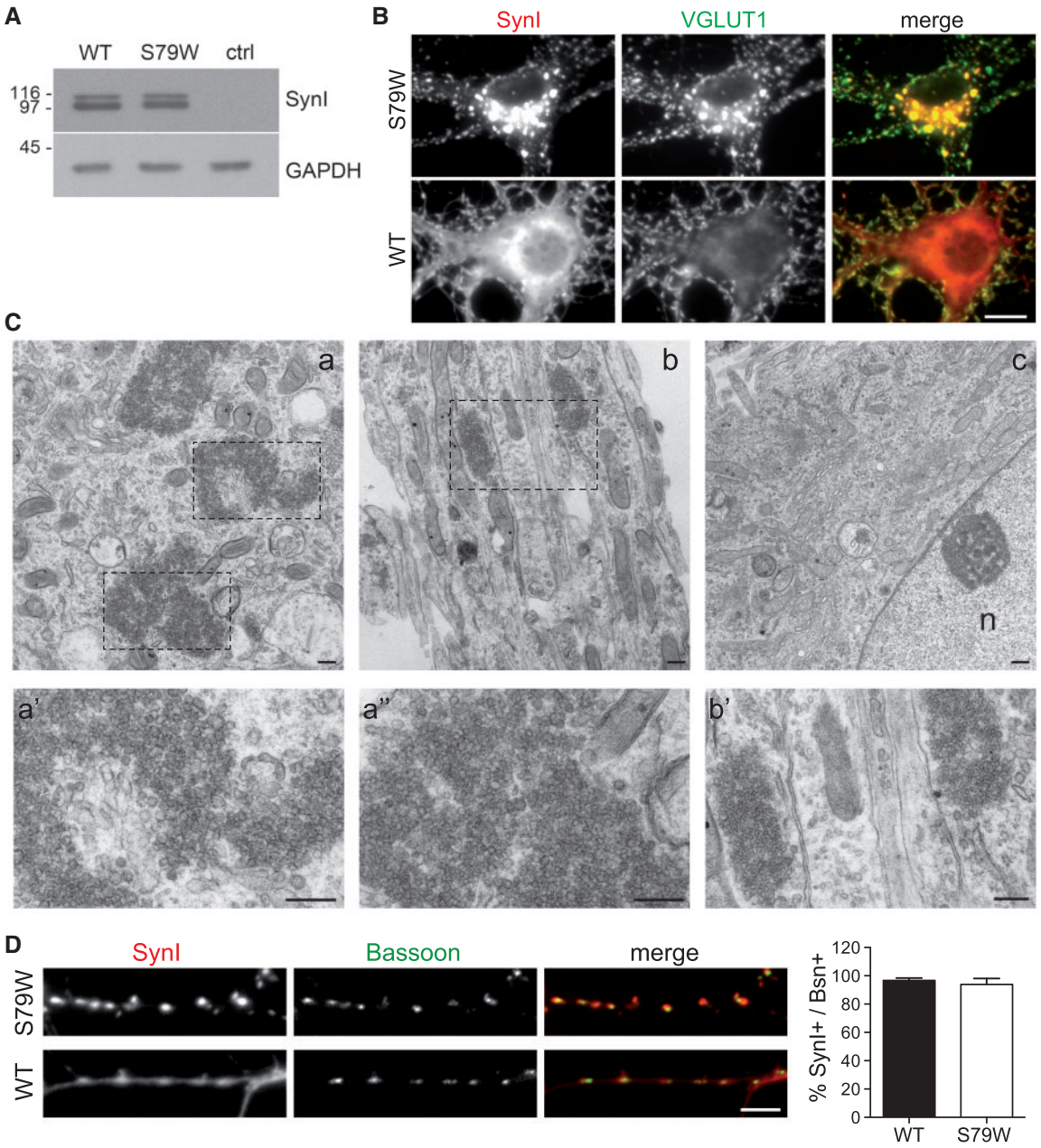


**Figure 4.** S79W SynI expression in hippocampal neurons leads to the formation of perinuclear aggregates composed of small clear vesicles. *Syn1* KO hippocampal neurons were infected at 10 DIV with lentiviral vectors coding for WT or S79W mCherry-tagged SynI and analysed at 17 DIV. (**A**) Representative Western Blot of transduced hippocampal neurons lysed in 1% SDS. mCherry-SynI expression was revealed with an anti-SynI antibody (G143). GAPDH (glyceraldehyde 3-phosphate dehydrogenase) was used as loading control. Ctrl: neurons transduced with lentiviruses coding for the mCherry tag. (**B**) Representative immunofluorescence images of cell soma of neurons expressing either WT or S79W mCherry-tagged SynI (red in *merge*panels), showing the presence of S79W SynI accumulations positive for the SV marker vesicular glutamate transporter 1 (VGLUT1, green in *merge* panels). Scale bar: 10 μm. (**C**) Transmission electron microscopy images showing accumulations of small clear vesicles at the cell soma (a) and along dendrites (b) of neurons expressing S79W SynI. Vesicle accumulations are not visible in neurons expressing WT SynI (c). The lower panels show higher magnifications of the areas highlighted in the upper panels. n: nucleus. Scale bars: 500 nm. (**D**) Representative immunofluorescence images of axon tracts of neurons expressing WT or S79W mCherry-tagged SynI. Cells were stained for the active zone scaffolding protein Bassoon. On the right, quantification of SynI targeting to *bona fide* presynaptic terminals is shown as percentage of Bassoon puncta double positive for SynI. Results are expressed as means ± SEM ($n = 3$ independent experiments; 10 axonal segments per conditions were analysed in each experiment; $P > 0.05$, unpaired Student's *t*-test). Scale bar: 5 μm.

excitatory terminals (i.e., asymmetric synapses), the density of SVs was significantly increased upon expression of S79W SynI as compared with WT SynI or mCherry (Fig.7A and B). In the same synapses, the mean nearest neighbour distance (MNND, i.e. the average distance between each vesicle and the nearest one) was significantly reduced (Fig. 7C). No difference was observed in the number of SVs docked at the active zone (Fig. 7D).

In inhibitory terminals (i.e., symmetric synapses), a slight but significant increase in the density of SVs was observed upon expression of S79W SynI (Fig. 7E and F). In the same synapses, MNND was significantly decreased (Fig. 7G), whereas the number of docked SVs was unaffected (Fig. 7H).

We also measured the density of excitatory synapses in neurons expressing either WT SynI, S79W SynI or mCherry by

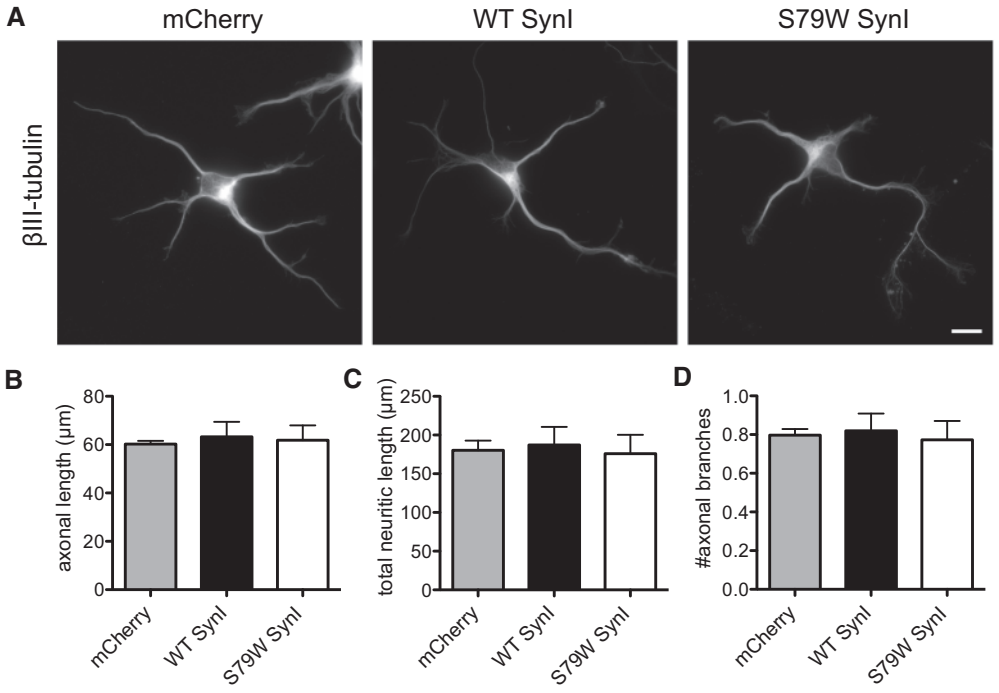


**Figure 5.** Neurite elongation is unaffected in young hippocampal neurons expressing S79W SynI. *Syn1* KO hippocampal neurons were electroporated at 0 DIV with plasmids coding for S79W or WT mCherry-tagged SynI or for the mCherry tag alone and analysed at 1.5 DIV. βIII-tubulin was used as a marker of neuronal cytoskeleton, in order to visualize the entire neuronal morphology. (**A**) Representative images of neurons expressing mCherry, WT SynI or S79W SynI (only βIII-tubulin signal is shown). Scale bar: 10 μm. (**B–D**) Quantification of axonal length and branches, total neuritic length, and number of axonal branches is shown. Results are expressed as means ± SEM ($n = 3$ independent experiments, 70–110 cells analysed per condition in each experiment; $P > 0.05$, one-way ANOVA followed by Tukey's multiple comparison test).

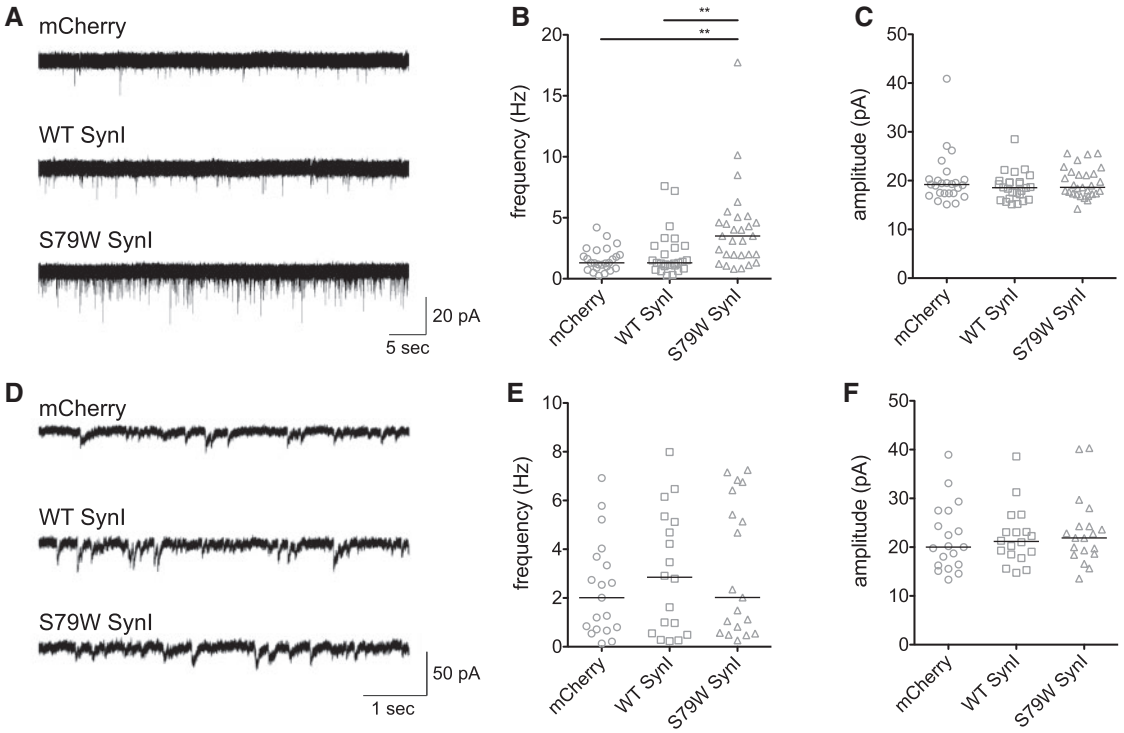


**Figure 6.** The expression of S79W Syn I increases mESPC, but not mIPSC, frequency in mature hippocampal neurons. *Syn1* KO hippocampal neurons were infected at 10 DIV with lentiviruses coding for WT or S79W mCherry-tagged SynI or for the mCherry tag alone. Whole-cell patch clamp recordings of mEPSCs and mIPSCs were performed at 16-17 DIV. (**A**) Representative traces of mEPSCs. (**B,C**) mEPSC frequency (B) and amplitude (C) are expressed as means ± SEM (mCherry $n = 25$, WT SynI $n = 26$, S79W SynI $n = 29$ neurons from 3 independent experiments; $^{**}P < 0.01$, Kruskal-Wallis followed by Dunn's multiple comparison test). (**D**) Representative traces of mIPSCs. (**E,F**) mIPSC frequency (E) and amplitude (F) are expressed as means ± SEM (mCherry $n = 19$, WT SynI $n = 18$, S79W SynI $n = 19$ neurons from 3 independent experiments; Kruskal-Wallis followed by Dunn's multiple comparison test).

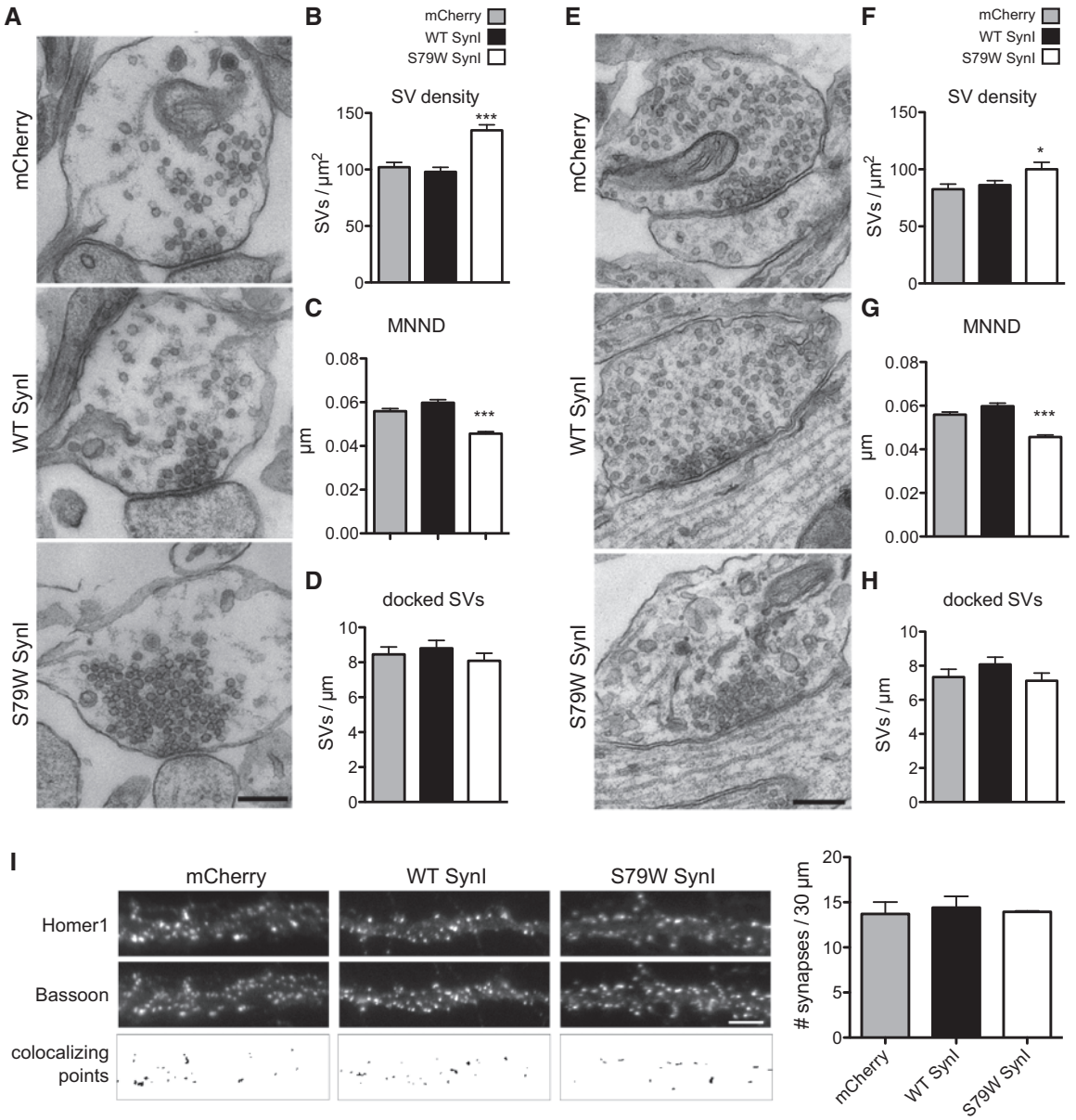


**Figure 7.** The expression of S79W SynI increases the density of SVs at presynaptic terminals, leaving synapse number unaffected. *Syn1* KO hippocampal neurons were infected at 10 DIV with lentiviruses coding for WT or S79W mCherry-tagged SynI or for the mCherry tag alone and analysed at 17 DIV. (**A**) Transmission electron microscopy images of representative excitatory presynaptic terminals from neurons expressing the mCherry tag, WT SynI or S79W SynI. Scale bar: 250 nm. (**B**) Density of SVs in excitatory presynaptic terminals (means ± SEM; mCherry $n = 62$, WT SynI $n = 68$, S79W SynI $n = 86$ synapses from 3 independent experiments; $^{***}P < 0.001$ S79W versus WT and mCherry; one-way ANOVA followed by Tukey's multiple comparison test). (**C**) Mean nearest neighbour distance (MNND) between SVs in excitatory terminals (means ± SEM; mCherry $n = 57$, WT SynI $n = 70$, S79W SynI $n = 76$ synapses from 3 independent experiments; $^{***}P < 0.001$ S79W versus WT and mCherry; Kruskal-Wallis followed by Dunn's multiple comparison test). (**D**) Density of SVs docked at the active zone in excitatory terminals (means ± SEM; mCherry $n = 55$, WT SynI $n = 63$, S79W SynI $n = 79$ synapses from 3 independent experiments; $P > 0.05$; one-way ANOVA followed by Tukey's multiple comparison test). (**E**) Transmission electron microscopy images of representative inhibitory presynaptic terminals from neurons expressing the mCherry tag or either WT or S79W mCherry-tagged SynI. Scale bar: 250 nm. (**F**) Density of SVs in inhibitory presynaptic terminals (means ± SEM; mCherry $n = 55$, WT SynI $n = 54$, S79W SynI $n = 58$ synapses from 3 independent experiments; $^{*}P < 0.05$ S79W versus mCherry; one-way ANOVA followed by Tukey's multiple comparison test). (**G**) Mean nearest neighbour distance (MNND) between SVs in inhibitory terminals (means ± SEM; mCherry $n = 51$, WT SynI $n = 54$, S79W SynI $n = 59$ synapses from three independent experiments; $^{***}P < 0.001$ S79W versus WT and mCherry; Kruskal-Wallis followed by Dunn's multiple comparison test). (**H**) Density of SVs docked at the active zone in inhibitory terminals (means ± SEM; mCherry $n = 50$, WT SynI $n = 51$, S79W SynI $n = 55$ synapses from 3 independent experiments; $P > 0.05$; one-way ANOVA followed by Tukey's multiple comparison test). (**I**) Number of excitatory synapses in neurons expressing the mCherry tag or either WT or S79W mCherry-tagged SynI. Synapses were counted on neurite segments of 30 µm as puncta of colocalization between the presynaptic marker Bassoon and the postsynaptic marker Homer1. Representative fluorescence images and colocalized puncta are shown in the left panel. Scale bar: 5 µm. Results from the quantification are shown on the right (means ± SEM; $n = 3$ independent experiments, at least 75 neurite segments analysed per condition in each experiment; $P > 0.05$, one-way ANOVA followed by Tukey's multiple comparison test).

immunofluorescence analyses; no significant difference was apparent among the three conditions (Fig. 7I).

### S79W SynI reduces the mobile pool of synaptic vesicles

In hippocampal neurons, the distribution of mCherry-tagged S79W SynI along axons was markedly different from that of the WT protein: S79W SynI appeared to be highly clustered at presynaptic terminals, while WT SynI was more diffused along axons. In the presence of S79W SynI, also the staining for endogenous VGLUT1 appeared highly clustered, whereas it was more dispersed along axons in neurons expressing WT SynI. The presynaptic scaffolding protein Bassoon, instead, appeared punctate in both conditions (Fig. 8A). To quantify this observation, we performed a mathematical analysis of SynI and VGLUT1 dispersion along axons (see Materials and Methods), by comparing neurons expressing WT or S79W SynI. The longitudinal, but not the transversal, dispersion of SynI and VGLUT1 signals was significantly reduced in neurons expressing S79W SynI as compared with neurons expressing WT SynI (Fig. 8B–E), indicating an increased clustering of SynI itself and of SVs at *bona fide* presynaptic terminals along the major axis of the axon.

The differential clustering of S79W SynI and of endogenous SVs prompted us to hypothesize that the mobility of S79W SynI itself and of S79W SynI-coated SVs could be altered, with possible implications for the dynamic spatial organization of SV clusters. To test this hypothesis, we performed fluorescence recovery after photobleaching (FRAP) experiments in *Syn1* KO hippocampal neurons expressing mCherry-tagged WT SynI or S79W SynI and a yellow fluorescent protein (YFP)-tagged version of the SV protein Syp. Photobleaching of SynI and Syp fluorescence was performed at single synaptic boutons and the dynamics of fluorescence recovery were monitored by time-lapse imaging (Fig. 8F and G). The rate of SynI recovery after bleaching was biexponential and displayed comparable kinetics in S79W or WT SynI expressing neurons. The asymptotic value of recovery was $37 \pm 2\%$ of the initial fluorescence for S79W SynI and $65 \pm 3\%$ for WT SynI ($P = 0.0016$, unpaired Student's *t*-test). The fast phase accounted for $23 \pm 4\%$ of the asymptotic recovery for S79W SynI and $41 \pm 3\%$ for WT SynI ($P = 0.024$, unpaired Student's *t*-test). These results indicate that S79W and WT SynI have comparable mobility kinetics, but the high-mobility fraction is significantly smaller for S79W than for WT SynI. Similarly, the rate of Syp recovery after bleaching was biexponential and displayed comparable kinetics in S79W or WT SynI expressing neurons. The fast phase accounted for $25 \pm 0.6\%$ of the asymptotic recovery for S79W SynI and $46 \pm 1\%$ for WT SynI ($P < 0.0001$, unpaired Student's *t*-test). The weight of the fast component on the fluorescence recovery was $17 \pm 2\%$ for S79W SynI and $12 \pm 2\%$ for WT SynI ($P = 0.22$, unpaired Student's *t*-test). These results indicate the presence of a significantly smaller pool of mobile SVs in presynaptic terminals expressing S79W SynI as compared with those expressing WT SynI, even though their mobility kinetics and their partitioning in fast- and slowly-moving pools were similar under the two conditions.

## Discussion

We identified a novel missense mutation (c.236 C > G/p.S79W) in the *SYN1* gene in the MRX50 family through a candidate-gene direct sequencing approach applied to a small number of families selected by linkage analysis. The family was classified as being affected by non-syndromic ID, i.e. characterized by a pure cognitive phenotype in the absence of other neurological deficits (20). Several mutations in the *SYN1* gene (p.Q555X, p.Q356X, p.A550T, p.T567A, p.A51G) have been identified in patients affected by epilepsy and/or autism (14,15). This is the first report indicating an involvement of SynI in the pathogenesis of non-syndromic ID. Thus, the detailed characterization of the cellular and functional effects of this specific mutation is important to elucidate the mechanisms that specifically lead to isolated ID rather than epilepsy.

The identified mutation is a single nucleotide substitution (c.236 C > G), which causes an amino acid change at the protein level (S79W). Ser-79 resides in domain B of SynI and is perfectly conserved along evolution, suggesting that this residue is important for the biological properties of the protein. Domain B contains an evolutionary conserved motif named ALPS (32), which allows SynI to sense membrane curvature and facilitates its association with SVs (23).

The ALPS peptide shows a random conformation in solution. The addition of highly curved liposomes mimicking the phospholipid composition and size (30–50 nm diameter) of SVs results in the folding of the motif as an amphipathic $\alpha$-helix, while no folding is induced when the peptide is incubated with larger liposomes. Deletion of the ALPS motif hampers the ability of SynI to recognize highly curved membranes and to cluster SVs *in vitro* (23). Ser-79 lies in the middle of the ALPS motif, which spans amino acids 69-96. We found that the expression of S79W SynI results in the accumulation of small clear vesicles in both HeLa cells and hippocampal neurons in culture. Thus, the S79W substitution seems to potentiate the ability of SynI to cluster SVs, possibly through an increased fitting to highly curved bilayers that could facilitate membrane budding processes. Interestingly, S79W SynI displays this aberrant property also when expressed in a heterologous system such as HeLa cells, indicating that the phenomenon does not require the presence of other synaptic interactors. The precise nature and origin of the small clear vesicles that accumulate in the perinuclear region of HeLa cells and hippocampal neurons expressing S79W SynI are difficult to figure out. We observed that these accumulations often reside in close proximity to the Golgi cisternae and that they colocalize with endogenous or exogenously expressed SV markers, suggesting that these organelles may represent SV precursors or intermediates deputed to SV protein sorting. Two possible explanations may be offered for these data: S79W SynI may be able either to promote the budding of new vesicles from Golgi membranes or to cluster pre-existing organelles.

ID is often associated with neurodevelopmental defects. Considering that synapsins have been linked to neuronal development and neurite extension (31), we evaluated whether S79W SynI interferes with these processes. The analysis of axonal and dendritic elongation in young hippocampal neurons expressing either WT or mutant SynI did not reveal any defect at the developmental stage analysed. Conversely, the Q555X mutation, identified in patients affected by epilepsy associated with learning disability and ASD, significantly impaired neurite extension when expressed in *Syn1* KO hippocampal neurons (15). This suggests that neurodevelopmental defects are not necessary to produce phenotypically isolated ID (not associated with epilepsy or ASD).

Despite the formation of somatic clusters, S79W SynI is transported to presynaptic terminals. We thus investigated the effects of the mutant protein on synaptic function and morphology in mature hippocampal neurons. Electrophysiological recordings showed that, as compared with neurons expressing

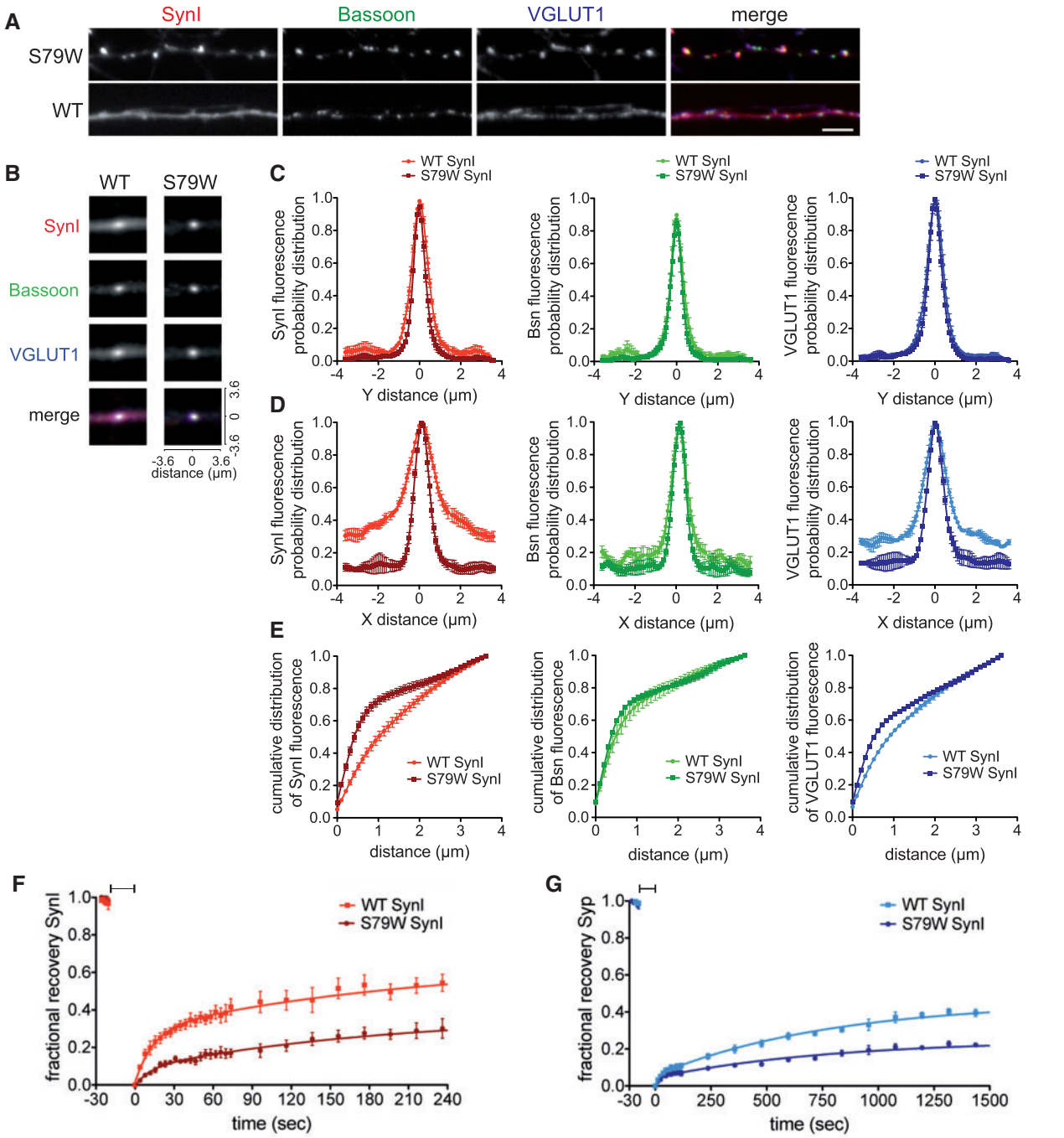


**Figure 8.** SVs are more clustered and less mobile along axons in neurons expressing S79W SynI. *Syn1* KO hippocampal neurons were infected at 10 DIV with lentiviruses coding for mCherry-tagged WT or S79W SynI and analysed at 17 DIV. For FRAP experiments, neurons were co-infected with lentiviruses coding for Syp-YFP. (**A**) Representative immunofluorescence images of isolated axonal segments marked with either S79W SynI or WT SynI (red), the presynaptic scaffolding protein Bassoon (green), and the vesicular protein VGLUT1 (blue). (**B–E**) Analysis of SynI, Bassoon and VGLUT1 dispersion along axons. Average fluorescence signals at single synaptic puncta for SynI, Bassoon (Bsn) or VGLUT1 are shown (B), as computed from axons of neurons expressing either WT SynI or S79W SynI, as indicated. Transversal (C) and longitudinal (D) probability distribution of fluorescence intensity are shown for the three channels, together with the cumulative probability distribution of fluorescence intensity along the longitudinal axis (E; mean ± SEM, $n = 3$ independent experiments, with 146 terminals analysed for WT SynI and 169 terminals analysed for S79W SynI). In B, D and E, note the higher dispersion of WT SynI along the longitudinal axis, as compared with S79W SynI. In neurons expressing WT SynI, also VGLUT1, but not Bassoon, appears more dispersed. The median displacement of SynI, Bassoon or VGLUT1 fluorescence intensity was calculated from the cumulative distributions shown in E. SynI displacement (average medians ± SEM): WT SynI = 1020 ± 93 nm, S79W SynI = 423 ± 35 ($P = 0.004$, Student's *t*-test). Bassoon displacement: WT SynI = 512 ± 78 nm, S79W SynI = 382 ± 13 ($P = 0.18$, Student's *t*-test). VGLUT1 displacement: WT SynI = 902 ± 31 nm, S79W SynI = 536 ± 21 ($P = 0.0006$, Student's *t*-test). (**F**) Fluorescence recovery curves after photobleaching of WT or S79W mCherry-tagged SynI. The bleaching phase is indicated by a bar at the top of the graph. $K_{fast}$ and $K_{slow}$ (± SEM): 5.4 ± 2.4 $min^{-1}$ and 0.3 ± 0.06 $min^{-1}$ for S79W SynI, and 4.8 ± 1.2 $min^{-1}$ and 0.3 ± 0.06 $min^{-1}$ for WT SynI (mean $\tau_{fast:}$ S79W = 11 s, WT = 13 s; mean $\tau_{slow:}$ S79W = 190 s, WT = 201 s; $P > 0.05$, unpaired Student's *t*-test). (**G**) Fluorescence recovery curves after photobleaching of Syp-YFP in neurons expressing either WT or S79W SynI. The bleaching phase is indicated by a bar at the top of the graph. $K_{fast}$ and $K_{slow}$ (± SEM): 3.6 ± 1.2 $min^{-1}$ and 0.072 ± 0.006 $min^{-1}$ for S79W SynI, and 4.2 ± 1.8 $min^{-1}$ and 0.078 ± 0.006 $min^{-1}$ for WT SynI (mean $\tau_{fast:}$ S79W = 16 s, WT = 14 s; mean $\tau_{slow:}$ S79W = 804 s, WT = 790 s; $P > 0.05$, unpaired Student's *t*-test).

WT SynI, neurons transduced with the S79W isoform have a higher frequency of mEPSCs, pointing to a presynaptic alteration. In agreement with this observation, the number of SVs clustered at presynaptic terminals in the presence of S79W SynI is significantly increased, while the number of synapses is unaffected by S79W SynI expression. Thus, S79W SynI probably increases spontaneous excitatory activity by positively affecting the number of SVs that are available for release in the excitatory terminal.

Spontaneous inhibitory transmission is not affected by S79W SynI expression, although SV density is slightly increased also in these terminals. This different behaviour may be ascribed to the higher frequency of spontaneous events that is typical of GABAergic terminals. Thus, these terminals are less sensitive to small increases in the number of SVs available. It is also noteworthy that SynI plays distinct roles at excitatory and inhibitory terminals, since its ablation differentially affects glutamatergic and GABAergic transmission (33). Indeed, an imbalance between excitation and inhibition has been postulated to be at the basis of the epileptic phenotype observed in *Syn* KO mice (18,33,34), and possibly also in human patients bearing *SYN1* mutations (35). Interestingly, excitation/inhibition imbalance and hyperexcitability of neuronal networks have been recently described in another example of XLID, namely fragile X syndrome (36–39).

Finally, we found that S79W SynI displays a decreased dispersion along axons than WT SynI. Consistently, SV markers are more efficiently clustered at *bona fide* synaptic boutons when S79W SynI is expressed. This result is in agreement with the reduction of the MNND measured in electron micrographs of presynaptic terminals. Functionally, this effect may have important implications in the dynamic regulation of SV recruitment upon stimulation, as it is possible that S79W SynI bears a higher affinity for SV membranes and detaches less easily upon stimulus-driven phosphorylation. Along this line, FRAP experiments indicate that S79W SynI has a reduced basal mobility along axons, suggesting that it is probably more stably anchored to SVs in presynaptic terminals. SVs themselves display a reduced mobility when S79W SynI is expressed, in agreement with the idea that SVs are more stably packed at presynaptic terminals and are less prone to travel along axons.

Sharing of SVs—belonging to the so-called "superpool"—between adjacent synapses is a well-known phenomenon (40–42), which participates in the modulation of synaptic strength and relative weight of each synapse as a functional basis for synaptic plasticity (43). Synapsins have been proposed to participate in the regulation of the SV superpool by restricting SV lateral mobility. The ablation of the three *Syn* genes in fact increases SV mobility along axons (44,45). In our experiments, S79W SynI is even more efficient than WT SynI in limiting SV lateral mobility between synapses. This may underlie important defects in establishing synaptic plastic modifications when S79W SynI is expressed.

In conclusion, we identified the c.236 C > G/p.S79W mutation in *SYN1* as causative for the non-syndromic ID of the MRX50 family. Accordingly, the *in vitro* characterization of S79W SynI clearly indicates that the mutation does not interfere with neurodevelopmental aspects, but perturbs spontaneous SV exocytosis, SV clustering and SV lateral mobility along axons. All these phenomena may severely impact on the dynamics of complex plasticity phenomena, thus affecting learning and memory and leading to the cognitive phenotype observed in MRX50 patients. The molecular and functional characteristics of the S79W SynI mutant are unique with respect to those exhibited by the identified SynI mutants associated with epilepsy and ASD. Future structure-function studies will be performed to identify which of the multiple SynI functions and molecular interactors are involved in the genesis of distinct phenotypes, i.e. epilepsy, ASD or ID.

## Materials and Methods

### Patients' selection and analysis of the *SYN1* gene

Twelve genomic DNA samples from males with XLID mapped to Xp11 were obtained from the repository of the European Mental Retardation Consortium in Nijmegen, The Netherlands. Control DNAs were from a previous collection of adult European males (46). For all individuals involved, the informed consent was obtained. The genomic organization of the *SYN1* gene (GenBank NC_000023) was analysed based on the Ensembl database (accession number ENSG00000008056). Primers were designed in order to amplify fragments of the gene covering the entire coding sequence and the proximal promoter region (570 bp from the ATG). PCR amplification was performed with the GoTaq Flexi DNA polymerase (Promega, Madison, WI, USA), according to manufacturer's instructions, on a GeneAmp PCR System 9700 instrument (Applied Biosystems-Life technologies, Monza, Italy). PCR products were purified before sequencing with the Exo-SAP-IT (Exonuclease I and Shrimp Alkaline Phosphatase) reagent (USB, Cleveland, Ohio, USA). Direct sequencing was performed with the BigDye Terminator v1.1 Cycle Sequencing kit (BDv1.1, Applied Biosystems), with the same forward and reverse primers used for amplification and, when needed, with additional internal primers. The products of the sequencing reactions were purified with Sephadex G50 Superfine (GE Healthcare, Buckinghamshire, UK) and loaded onto MultiScreen HV 96-well plates (Millipore, Vimodrone, Italy). Samples were analysed in an ABI-3730 DNA Analyzer (Applied Biosystems). Sequences were manually verified through alignment with the reference sequence using ClustalW and BLASTN. A full list of primers used is reported in Supplementary Material, Table S2. The mutation identified (c.236 C > G/S79W) has been submitted to the LSDB database (https://databases.lovd.nl/shared/genes/SYN1; date last accessed September 15, 2017).

### Animals

Mice were housed under constant temperature (22 ± 1 °C) and humidity (50%) conditions with a 12 h light/dark cycle, and were provided with food and water *ad libitum*. *Syn1* KO mice (47) were used for generating primary neuronal cultures. All animal manipulations followed the guidelines established by the European Community Council (Directive 2010/63/EU of September 22nd, 2010) and were approved by the Institutional Animal Care and Use Committee (IACUC, permission number 467 and 565) of the San Raffaele Scientific Institute and by the Italian Ministry of Health. All efforts were made to minimize animal suffering.

### Plasmids and lentiviral vectors

The mCherry-tagged human WT *SYN1* (isoform Ia, NM_006950) construct was kindly provided by Dr. Anna Fassio (Department of Experimental Medicine, University of Genoa, Genoa, Italy) (15). The FLAG-tagged version has been previously generated (30). Non-tagged human WT *SYN1* was obtained by subcloning the cDNA into the pCAG-IRES-tdTomato plasmid, kindly provided by Dr. Laura Cancedda (Istituto Italiano di Tecnologia,

Genoa, Italy) (48). The missense mutations c.236 C > G (S79W) and c.235 T > G (S79A) were inserted in the mCherry- and FLAG-tagged WT *SYN1* constructs by site-directed mutagenesis (QuikChange Lightning Mutagenesis Kit, Agilent Technologies) using the following primers: human S79W_for GTGGCTT CTTCTCGTGGCTGTCCAACGCG; human S79W_rev CGCGTTGG ACAGCCACGAGAAGAAGCCAC; human S79A_for GTGGCTTCTT CTCGGCGCTGTCCAACGCG; human S79A_rev CGCGTTGGACAG CGCCGAGAAGAAGCCAC. The pCMV6-m*Syn1a* plasmid, coding for mouse WT SynI, was purchased from Origene (Rockville, MD, USA). The same missense mutations (c.236 C > G and c.235 T > G) were inserted by site-directed mutagenesis (QuikChange Lightning Mutagenesis Kit, Agilent Technologies) using the following primers: mouse S79W_for GCGGCTTCTTC TCGTGGCTGTCTAACGCG; mouse S79W_rev CGCGTTAGACAG CCACGAGAAGAAGCCGC; mouse S79A_for GCGGCTTCTTCTCGG CGCTGTCTAACGCG; mouse S79A_rev CGCGTTAGACAGCGCCG AGAAGAAGCCGC. The plasmid coding for synaptophysin-ECFP (Syp-ECFP) has been previously generated (49). Lentiviral vectors were produced by cloning the mCherry-tagged WT or S79W SynI or mCherry alone into the p743.pCCLsin.PPT.hPGK.GFP.Wpre vector provided by Dr. Luigi Naldini (San Raffaele Scientific Institute, Milan, Italy). Lentiviral vector for Syp-YFP has been previously generated (50). Viral stocks were produced as previously described (44,51). All reagents used for cloning were from New England Biolabs (NEB, Ipswich, MA, USA).

## Cell culture procedures

Primary neuronal cultures were prepared from the hippocampi of embryonic day 17.5 embryos from *Syn1* KO mice of either sex, as previously described (44). Neurons were plated on poly-L-lysine (0.1 mg/ml; Sigma-Aldrich, Milan, Italy)-coated 24 mm glass at a density of 150, 000 cells per coverslip, and maintained as a sandwich co-culture with astroglia in Modified Eagle's Medium (MEM; Invitrogen, Carlsbad, CA, USA) supplemented with 1% N2 supplement (Invitrogen), 2 mM glutamine (Invitrogen), 1 mM sodium pyruvate (Sigma-Aldrich, Milan, Italy), and 4 mM glucose, at 37 °C in 5% $CO_2$ humidified atmosphere.

For lentiviral transduction, coverslips were placed in a clean dish containing a mixture of fresh and conditioned medium, and were incubated overnight in the presence of viral stocks at a multiplicity of infection of 2-3. After transduction, neurons were returned to the original dishes and maintained in culture until analysis. For all experiments, neurons were infected at 10 DIV and analysed after one week, at 16-18 DIV.

Electroporation of neuronal cells was performed immediately after mechanical dissociation of the hippocampi with the Basic Primary Neurons Nucleofector Kit (Lonza, Basel, Switzerland) and the Amaxa Nucleofector Device (Amaxa Biosystems, Cologne, Germany), according to manufacturer's instructions (1 million cells and 3 μg of DNA/condition; O-05 program).

HeLa cells were grown in Dulbecco's Modified Eagle's Medium (DMEM; Invitrogen) supplemented with 10% foetal clone III serum (FCIII; Celbio, Pero, Italy), 1% glutamine and 1% penicillin/streptomycin (P/S; Invitrogen), at 37 °C in 5% $CO_2$ humidified atmosphere.

Transient transfection of HeLa cells was performed with Lipofectamine-2000 (Invitrogen), following manufacturer's instructions.

## Cell labelling, image acquisition and analysis

Immunofluorescence experiments were performed as previously described (44). Briefly, cells were rinsed once with Krebs–Ringer's solution (KRH)–EGTA (in mM: 130 NaCl, 5 KCl, 1.2 $KH_2PO_4$, 1.2 $MgSO_4$, 2 $MgCl_2$, 2 EGTA, 25 Hepes, and 6 glucose, pH 7.4), fixed for 15 min with 4% paraformaldehyde, 4% sucrose in 120 mM sodium phosphate buffer, pH 7.4, supplemented with 2 mM EGTA. Coverslips were rinsed three times with phosphate buffer saline (PBS) and then incubated overnight at 4 °C in a humidified chamber with the primary antibody appropriately diluted in goat serum dilution buffer (GSDB; 15% goat serum, 450 mM NaCl, 0.3% Triton X-100, and 20 mM sodium phosphate buffer, pH 7.4). Specimens were then washed three times with PBS and incubated with the appropriate secondary antibody for 1 h at RT. After three washes with PBS, coverslips were mounted with the Dako fluorescence mounting medium (Dako North America, Carpinteria, CA, USA). Primary antibodies: SynI rabbit (G143) 1: 200 home-made (52); FLAG-tag rabbit 1: 400 (Sigma-Aldrich); VGLUT1 rabbit 1: 200 (Synaptic Systems, Goettingen, Germany); βIII-tubulin mouse 1: 1000 (Promega); Bassoon mouse 1: 150 (Stressgen – Enzo Life Sciences, Farmingdale, NY, USA); Homer1 rabbit 1: 200 (Synaptic Systems); GM130 mouse 1: 300 (BD Biosciences, Franklin Lakes, NJ, USA). Secondary antibodies: FITC anti-mouse 1: 50 (Jackson ImmunoResearch, West Grove, PA, USA), Alexa-647 anti-rabbit 1: 100 (Invitrogen). When indicated, nuclei staining was performed by incubating coverslips with the Hoechst 33342 dye (ThermoFisher, Waltham, MA, USA) diluted 1: 10000 in PBS for 5 min during the last round of washes. FITC-conjugated phalloidin (Sigma-Aldrich) was added during incubation of the secondary antibodies (diluted 1: 100), when indicated. Epifluorescence images were acquired with an inverted microscope (Axiovert 135; Carl Zeiss, Oberkochen, Germany) equipped with a 63X objective. Images were recorded with a C4742-98 ORCA II cooled charge-coupled device camera. Image analysis was performed with ImageJ and specific plugins. In particular, the analysis of SynI synaptic targeting was performed on axonal segments of 30 μm by automatically selecting circular ROIs of 1 μm-diameter on Bassoon puncta and counting the number of ROIs displaying red fluorescence above a constant threshold (SynI). Neurite elongation was measured with the NeuronJ plugin. βIII-tubulin was used as a marker of neuronal cytoskeleton, and axons were recognized based on morphological criteria. Synapse count was performed on neurite segments of 30 μm adjacent to cell soma, with the Colocalization Highlighter plugin by selecting and counting points of colocalization between a presynaptic (Bassoon) and an excitatory postsynaptic marker (Homer1) in the range of 0.1–1 $\mu m^2$. SynI and SV dispersion along axons was analysed by locating about 50 Bassoon puncta (range: 47–58) in each experiment, and adding up the images of the surrounding areas, centred on the highest intensity pixel of each spot ("centre-pixel"). The resulting three-chromic images (red = SynI, green = Bassoon, blue = VGLUT1) were displayed to offer a visual perception of the colocalization. The distribution of the proteins was analysed by measuring the light intensity in the three channels along the lines that crossed at the centre-pixel, parallel and orthogonal to the major axis of the neurite. To quantitatively compare the displacement of the markers, cumulative histograms were plotted and the median distance from the centre-pixel was computed. To perform these analyses, original software was developed in Matlab R2011a environment (The MatWorks, Natick, MA).

## Fluorescence recovery after photobleaching (FRAP)

Live neurons were imaged in KRH buffer (in mM: 130 NaCl, 5 KCl, 1.2 $KH_2PO_4$, 1.2 $MgSO_4$, 2 $CaCl_2$, 25 Hepes, and 6 glucose, pH

7.4, 310 mOsm). Imaging was performed on a Leica TCS SP8 laser scanning confocal microscope equipped with a 63X/1.4 NA oil immersion objective and a stage incubator with temperature and $CO_2$ control. Images were acquired at 2.5X zoom, 512×512 pixels, 400 Hz speed, 1 line and frame average. For mCherry-SynI FRAP, images were acquired with the 522 nm laser line of a white laser at 8% laser power, with 623.3 V gain, -0.3% offset and 2.5 pinhole. Bleaching was performed with the 552 nm and 561 nm laser lines at 100% power. Ten images were acquired for pre-bleaching signal determination at 1.29 s intervals. Bleaching was performed with 15 pulses on 6 circular regions of interest (ROIs)/field (ROI area: 3 $\mu m^2$ on average), designed to bleach single *bona fide* synaptic boutons. After bleaching, 60 images were acquired at 1.29 s intervals followed by 25 images at 20 s intervals to monitor fluorescence recovery over time. For Syp-YFP FRAP, images were acquired with the 488 nm laser line of an Argon laser at 3% laser power, with 750 V gain, 0% offset and 2.5 pinhole. Bleaching was performed with the 488 nm laser lines at 50% power. Ten images were acquired for pre-bleaching signal determination at 1.29 s intervals. Bleaching was performed with 15 pulses on 6 circular regions of interest (ROIs)/field (ROI area: 3 $\mu m^2$ on average) on single *bona fide* synaptic boutons double positive for Syp-YFP and mCherry-SynI. After bleaching, 40 images were acquired at 3 s intervals followed by 20 images at 2 min intervals to monitor fluorescence recovery over time. Images were corrected for drift, but not for bleaching, with NIH ImageJ. Focal drift was automatically corrected by the autofocus function of the microscope. For quantitative analysis of fluorescence recovery at each ROI, data were double normalized as described previously (53). Double exponential fits of FRAP curves were obtained with GraphPad Prism (La Jolla, CA, USA).

## Western blotting

Neuronal cells were lysed with a buffer containing 1% sodium dodecylsulfate (SDS), 10 mM HEPES, 2 mM EDTA pH 7.4. Protein content was quantified with bicinchoninic acid assay (BCA, ThermoFisher). Laemmli buffer was added to a final 1X concentration (20 mM Tris pH 6.8, 2 mM EDTA, 2% SDS, 10% glycerol, 2% β-mercaptoethanol 0.01% bromophenol blue). Equal protein amounts were loaded on a polyacrylamide gel, subjected to standard SDS-PAGE, using a Standard Vertical Gel Electrophoresis unit (Hoefer, San Francisco, CA, USA), and transferred to a nitrocellulose membrane (Whatman GmbH, Dassel, Germany). Blocking of the membranes was performed in 5% milk-TBST (Tris-Base saline-Tween: 150 mM NaCl, 20 mM Tris-HCl pH 7.4, 0.05% Tween 20) for 1 h at room temperature (RT). Primary antibodies were appropriately diluted in 5% milk-TBST and incubated overnight at 4° C in a humidified chamber. Membranes were washed three times in TBST to eliminate primary antibody in excess. Secondary horseradish peroxidase (HRP)-conjugated anti-mouse and anti-rabbit antibodies (1: 10000, BioRad Cat#170-6516/6515 RRID: AB_11125547 RRID: AB_11125142, Hercules, CA, USA) were diluted in 5% milk-TBST and incubated for 1 h at RT. Membranes were washed three times in TBST to remove secondary antibodies in excess. Detection was performed with the enhanced chemiluminescence reaction (ECL; Amersham-GE Healthcare, Buckinghamshire, UK). Signals were visualized on ECL Hyperfilms (Amersham) and scanned with a desktop scanner (Epson Perfection V800 Photo) at 600 dpi. Primary antibodies used: mouse anti-Syn G143 (1: 5000, home-made) (52), rabbit anti-GAPDH (glyceraldehyde-3-phosphate dehydrogenase; 1: 10000, Cell Signaling Technology, Danvers, MA, USA); mouse anti-β-actin (1: 5000, Sigma-Aldrich).

Triton X-100 solubility of WT and S79W SynI was assessed as previously described (54). Briefly, HeLa cells plated on 35 mm Petri dishes were transfected with FLAG-tagged constructs. After 48 h, cells were harvested and resuspended with 100 µl of a solution containing 10 mM Tris-HCl pH 7.4, 1 mM EDTA. The samples were then lysed with an equal volume of 2% Triton X-100 in the same Tris-EDTA buffer. Lysates were rotated on a wheel for 30 min at 4 °C, then 50 µl were removed for the analysis of the total lysate, and the remaining lysates were centrifuged at 12, 000 g for 10 min. After withdrawal of the supernatants, the pellets were resuspended in 75 µl of 10 mM Tris-HCl pH 7.4, and treated with DNase (40 mg/ml final concentration) to digest any released DNA. The resuspended pellets were then brought to 150 µl, and equal volumes of the total lysates, pellets and supernatants were analysed by SDS-PAGE and Western blotting. All solutions contained a protease inhibitor cocktail (Sigma-Aldrich).

## Electrophysiological recordings

Patch-clamp recordings were performed in an extracellular solution with the following composition (in mM): 130 NaCl, 5 KCl, 1.2 $KH_2PO_4$, 1.2 $MgSO_4$, 2 $CaCl_2$, 25 Hepes, and 6 glucose, pH 7.4, with glass pipettes of 4-6 MΩ as recording electrodes. mEPSCs were recorded in the presence of bicuculline (20 µM), (2 R)-amino-5-phosphonovaleric acid (APV; 50 µM) and tetrodotoxin (TTX; 1 mM) using the following internal solution (in mM): 135 K-gluconate, 5 KCl, $MgCl_2$, 10 Hepes, 1 EGTA, 2 ATP, 0.5 GTP, pH 7.4. mIPSCs were recorded in the presence of 6-cyano-7-nitroquinoxaline-2, 3-dione (CNQX; 20 µM), APV (50 µM) and TTX (1 mM) using the following internal solution (in mM): 68 K-gluconate, 68 KCl, 2 $MgSO_4$, 20 Hepes, 2 ATP, 0.5 GTP, pH 7.2. Both mEPSCs and mIPSCs were recorded at -70 mV holding potential. Electrical signals were amplified by a Multiclamp 200 B (Axon instruments, Union City, CA, USA), filtered at 5 kHz, digitized at 20 kHz with a digidata 1440 and stored with pClamp 10 (Axon instruments). The resting potential was measured at $I = 0$ in current clamp configuration, whereas input resistance was calculated in voltage clamp configuration by using the slope of the I/V relationship of the steady state current measured at different hyperpolarizing voltage steps (from -100 to -70 mV). Infected cells were visualized using a LED-based illumination system (Cairn Research, Optoled, Faversham, UK). Only cells with an access resistance $<20$ MΩ were considered for the analysis. Access resistance was continuously monitored during the experiment and those cells in which access resistance was changed by more than 10% were rejected. The analysis of both mEPSC and mIPSC was performed with Mini analysis (Synaptosoft Inc., Fort Lee, NJ, USA).

## Transmission electron microscopy

Primary hippocampal neurons were fixed with 1.3% glutaraldehyde in 66 mM sodium cacodylate buffer (pH 7.4), postfixed in 1% OsO4, 1.5% $K_4Fe(CN)_6$, 0.1 M sodium cacodylate, *en bloc* stained with 0.5% uranyl acetate, dehydrated and embedded in Epon. Ultrathin sections were contrasted with 2% uranyl acetate and Sato's lead solution (55), observed with a LEO 912AB (Zeiss, Oberkochen, Germany) transmission electron microscope operated at 80 kV. Images were taken with a ProScan 2048x2048 pixel Slow-Scan CCD camera (ProScan, Lagerlechfeld, Germany) controlled by EsiVision 3.2 software (Soft-Imaging Software, Münster, Germany). Morphometric analysis of cross-section

synaptic areas, total and docked SVs was performed in ImageJ. For the analysis of the spatial distribution of SVs, the position of each SV was located in ImageJ and the coordinates were transferred to Crimestat (Ned Levine; 2010, Houston, TX, USA) where the distance from the closest SV (mean nearest neighbour distance, MNND) was calculated.

### Statistical analysis

Data were analysed using Microsoft Excel and Prism 5.0 software (GraphPad, La Jolla, CA, USA). Normality of data distributions was calculated using a Kolmogorov–Smirnov test. According to normality, data comparisons were computed using either unpaired Student's *t*-test or Mann-Whitney U-test in case of comparisons between two groups, and either one-way ANOVA followed by Tukey's multiple comparison test or Kruskal-Wallis test followed by the Dunn's multiple comparison test in case of comparisons between more than two groups.

## Supplementary Material

Supplementary Material is available at *HMG* online.

## Acknowledgements

The authors would like to acknowledge Dr. Elena Monzani for technical assistance, Dr Eugenio Fornasiero (ENI, Goettingen, Germany) for helpful advice, Dr Anna Fassio (University of Genoa, Italy), Dr Laura Cancedda (Istituto Italiano di Tecnologia, Genoa, Italy) and Dr Luigi Naldini (San Raffaele Scientific Institute, Milan, Italy) for providing plasmidic constructs. ALEMBIC (the Advanced Light and Electron Microscopy Bioimaging Center of the San Raffaele Scientific Institute) provided the facilities for performing part of the experiments.

*Conflict of Interest statement*. None declared.

## Funding

Jerome Lejeune Foundation (grant number 953-VF2011B to F.V.), Telethon (grant number GGP13033 to F.V. and F.B.) and Italian Ministry for University and Research (grant PRIN 2015H4K2CR to F.B. and F.V.). H.V.E. is a clinical investigator of FWO Vlaanderen.

## References

1. American Psychiatric Association. (2013) *Diagnostic and Statistical Manual of Mental Disorders (5th ed.)*, Washington, DC.
2. Maulik, P.K., Mascarenhas, M.N., Mathers, C.D., Dua, T. and Saxena, S. (2011) Prevalence of intellectual disability: a meta-analysis of population-based studies. *Res. Dev. Disabil.*, **32**, 419–436.
3. Brereton, A.V., Tonge, B.J. and Einfeld, S.L. (2006) Psychopathology in children and adolescents with autism compared to young people with intellectual disability. *J. Autism Dev. Disord.*, **36**, 863–870.
4. Matson, J.L. and Shoemaker, M. (2009) Intellectual disability and its relationship to autism spectrum disorders. *Res. Dev. Disabil.*, **30**, 1107–1114.
5. Ropers, H.H. (2010) Genetics of early onset cognitive impairment. *Annu. Rev. Genomics Hum. Genet.*, **11**, 161–187.
6. Gilissen, C., Hehir-Kwa, J.Y., Thung, D.T., van de Vorst, M., van Bon, B.W., Willemsen, M.H., Kwint, M., Janssen, I.M., Hoischen, A., Schenck, A. *et al.* (2014) Genome sequencing identifies major causes of severe intellectual disability. *Nature*, **511**, 344–347.
7. Chiurazzi, P. and Pirozzi, F. (2016) Advances in understanding - genetic basis of intellectual disability. *F1000Res*, **5**,
8. van Bokhoven, H. (2011) Genetic and epigenetic networks in intellectual disabilities. *Annu. Rev. Genet.*, **45**, 81–104.
9. Saitsu, H., Kato, M., Mizuguchi, T., Hamada, K., Osaka, H., Tohyama, J., Uruno, K., Kumada, S., Nishiyama, K., Nishimura, A. *et al.* (2008) De novo mutations in the gene encoding STXBP1 (MUNC18-1) cause early infantile epileptic encephalopathy. *Nat. Genet.*, **40**, 782–788.
10. D'Adamo, P., Menegon, A., Lo Nigro, C., Grasso, M., Gulisano, M., Tamanini, F., Bienvenu, T., Gedeon, A.K., Oostra, B., Wu, S.K. *et al.* (1998) Mutations in GDI1 are responsible for X-linked non-specific mental retardation. *Nat. Genet.*, **19**, 134–139.
11. Borck, G., Wunram, H., Steiert, A., Volk, A.E., Korber, F., Roters, S., Herkenrath, P., Wollnik, B., Morris-Rosendahl, D.J. and Kubisch, C. (2011) A homozygous RAB3GAP2 mutation causes Warburg Micro syndrome. *Hum. Genet.*, **129**, 45–50.
12. Aligianis, I.A., Johnson, C.A., Gissen, P., Chen, D., Hampshire, D., Hoffmann, K., Maina, E.N., Morgan, N.V., Tee, L., Morton, J. *et al.* (2005) Mutations of the catalytic subunit of RAB3GAP cause Warburg Micro syndrome. *Nat. Genet.*, **37**, 221–223.
13. Aligianis, I.A., Morgan, N.V., Mione, M., Johnson, C.A., Rosser, E., Hennekam, R.C., Adams, G., Trembath, R.C., Pilz, D.T., Stoodley, N. *et al.* (2006) Mutation in Rab3 GTPase-activating protein (RAB3GAP) noncatalytic subunit in a kindred with Martsolf syndrome. *Am. J. Hum. Genet.*, **78**, 702–707.
14. Garcia, C.C., Blair, H.J., Seager, M., Coulthard, A., Tennant, S., Buddles, M., Curtis, A. and Goodship, J.A. (2004) Identification of a mutation in synapsin I, a synaptic vesicle protein, in a family with epilepsy. *J. Med. Genet.*, **41**, 183–186.
15. Fassio, A., Patry, L., Congia, S., Onofri, F., Piton, A., Gauthier, J., Pozzi, D., Messa, M., Defranchi, E., Fadda, M. *et al.* (2011) SYN1 loss-of-function mutations in autism and partial epilepsy cause impaired synaptic function. *Hum. Mol. Genet.*, **20**, 2297–2307.
16. Corradi, A., Fadda, M., Piton, A., Patry, L., Marte, A., Rossi, P., Cadieux-Dion, M., Gauthier, J., Lapointe, L., Mottron, L. *et al.* (2014) SYN2 is an autism predisposing gene: loss-of-function mutations alter synaptic vesicle cycling and axon outgrowth. *Hum. Mol. Genet.*, **23**, 90–103.
17. Cesca, F., Baldelli, P., Valtorta, F. and Benfenati, F. (2010) The synapsins: key actors of synapse function and plasticity. *Prog. Neurobiol.*, **91**, 313–348.
18. Fassio, A., Raimondi, A., Lignani, G., Benfenati, F. and Baldelli, P. (2011) Synapsins: from synapse to network hyperexcitability and epilepsy. *Semin. Cell Dev. Biol.*, **22**, 408–415.
19. Valtorta, F., Pozzi, D., Benfenati, F. and Fornasiero, E.F. (2011) The synapsins: multitask modulators of neuronal development. *Semin. Cell Dev. Biol.*, **22**, 378–386.
20. Claes, S., Vogels, A., Holvoet, M., Devriendt, K., Raeymaekers, P., Cassiman, J.J. and Fryns, J.P. (1997) Regional localization of two genes for nonspecific X-linked mental retardation to Xp22.3-p22.2 (MRX49) and Xp11.3-p11.21 (MRX50). *Am. J. Med. Genet.*, **73**, 474–479.
21. de Brouwer, A.P., Yntema, H.G., Kleefstra, T., Lugtenberg, D., Oudakker, A.R., de Vries, B.B., van Bokhoven, H., Van Esch, H., Frints, S.G., Froyen, G. *et al.* (2007) Mutation frequencies of X-linked mental retardation genes in families from the EuroMRX consortium. *Hum. Mutat.*, **28**, 207–208.

22. Sudmant, P.H., Rausch, T., Gardner, E.J., Handsaker, R.E., Abyzov, A., Huddleston, J., Zhang, Y., Ye, K., Jun, G., Hsi-Yang Fritz, M. *et al.* (2015) An integrated map of structural variation in 2, 504 human genomes. *Nature*, **526**, 75–81.
23. Krabben, L., Fassio, A., Bhatia, V.K., Pechstein, A., Onofri, F., Fadda, M., Messa, M., Rao, Y., Shupliakov, O., Stamou, D. *et al.* (2011) Synapsin I senses membrane curvature by an amphipathic lipid packing sensor motif. *J. Neurosci.*, **31**, 18149–18154.
24. Adzhubei, I., Jordan, D.M. and Sunyaev, S.R. (2013) Predicting functional effect of human missense mutations using PolyPhen-2. *Curr. Protoc. Hum. Genet.*, **Chapter 7**, Unit7 20.
25. Jovanovic, J.N., Sihra, T.S., Nairn, A.C., Hemmings, H.C., Jr., Greengard, P. and Czernik, A.J. (2001) Opposing changes in phosphorylation of specific sites in synapsin I during Ca2+-dependent glutamate release in isolated nerve terminals. *J. Neurosci.*, **21**, 7944–7953.
26. Matsubara, M., Kusubata, M., Ishiguro, K., Uchida, T., Titani, K. and Taniguchi, H. (1996) Site-specific phosphorylation of synapsin I by mitogen-activated protein kinase and Cdk5 and its effects on physiological functions. *J. Biol. Chem.*, **271**, 21108–21113.
27. Skorobogatko, Y., Landicho, A., Chalkley, R.J., Kossenkov, A.V., Gallo, G. and Vosseller, K. (2014) O-linked beta-N-acetylglucosamine (O-GlcNAc) site thr-87 regulates synapsin I localization to synapses and size of the reserve pool of synaptic vesicles. *J. Biol. Chem.*, **289**, 3602–3612.
28. Steentoft, C., Vakhrushev, S.Y., Joshi, H.J., Kong, Y., Vester-Christensen, M.B., Schjoldager, K.T., Lavrsen, K., Dabelsteen, S., Pedersen, N.B., Marcos-Silva, L. *et al.* (2013) Precision mapping of the human O-GalNAc glycoproteome through SimpleCell technology. *Embo J.*, **32**, 1478–1488.
29. Blom, N., Sicheritz-Ponten, T., Gupta, R., Gammeltoft, S. and Brunak, S. (2004) Prediction of post-translational glycosylation and phosphorylation of proteins from the amino acid sequence. *Proteomics*, **4**, 1633–1649.
30. Giannandrea, M., Guarnieri, F.C., Gehring, N.H., Monzani, E., Benfenati, F., Kulozik, A.E., Valtorta, F. and Gonzalez-Alegre, P. (2013) Nonsense-mediated mRNA decay and loss-of-function of the protein underlie the X-linked epilepsy associated with the W356x mutation in synapsin I. *PLoS One*, **8**, e67724.
31. Fornasiero, E.F., Bonanomi, D., Benfenati, F. and Valtorta, F. (2010) The role of synapsins in neuronal development. *Cell. Mol. Life Sci.*, **67**, 1383–1396.
32. Antonny, B. (2011) Mechanisms of membrane curvature sensing. *Annu. Rev. Biochem.*, **80**, 101–123.
33. Chiappalone, M., Casagrande, S., Tedesco, M., Valtorta, F., Baldelli, P., Martinoia, S. and Benfenati, F. (2009) Opposite changes in glutamatergic and GABAergic transmission underlie the diffuse hyperexcitability of synapsin I-deficient cortical networks. *Cereb. Cortex*, **19**, 1422–1439.
34. Gitler, D., Takagishi, Y., Feng, J., Ren, Y., Rodriguiz, R.M., Wetsel, W.C., Greengard, P. and Augustine, G.J. (2004) Different presynaptic roles of synapsins at excitatory and inhibitory synapses. *J. Neurosci.*, **24**, 11368–11380.
35. Lignani, G., Raimondi, A., Ferrea, E., Rocchi, A., Paonessa, F., Cesca, F., Orlando, M., Tkatch, T., Valtorta, F., Cossette, P., Baldelli, P. and Benfenati, F. (2013) Epileptogenic Q555X SYN1 mutant triggers imbalances in release dynamics and short-term plasticity. *Hum. Mol. Genet.*, **22**, 2186–2199.
36. Gibson, J.R., Bartley, A.F., Hays, S.A. and Huber, K.M. (2008) Imbalance of neocortical excitation and inhibition and altered UP states reflect network hyperexcitability in the mouse model of fragile X syndrome. *J. Neurophysiol.*, **100**, 2615–2626.
37. Olmos-Serrano, J.L., Paluszkiewicz, S.M., Martin, B.S., Kaufmann, W.E., Corbin, J.G. and Huntsman, M.M. (2010) Defective GABAergic neurotransmission and pharmacological rescue of neuronal hyperexcitability in the amygdala in a mouse model of fragile X syndrome. *J. Neurosci.*, **30**, 9929–9938.
38. Patel, A.B., Hays, S.A., Bureau, I., Huber, K.M. and Gibson, J.R. (2013) A target cell-specific role for presynaptic Fmr1 in regulating glutamate release onto neocortical fast-spiking inhibitory neurons. *J. Neurosci.*, **33**, 2593–2604.
39. Bianchi, R., Chuang, S.C., Zhao, W., Young, S.R. and Wong, R.K. (2009) Cellular plasticity for group I mGluR-mediated epileptogenesis. *J. Neurosci.*, **29**, 3497–3507.
40. Staras, K., Branco, T., Burden, J.J., Pozo, K., Darcy, K., Marra, V., Ratnayaka, A. and Goda, Y. (2010) A vesicle superpool spans multiple presynaptic terminals in hippocampal neurons. *Neuron.* **66**, 37–44.
41. Darcy, K.J., Staras, K., Collinson, L.M. and Goda, Y. (2006) Constitutive sharing of recycling synaptic vesicles between presynaptic boutons. *Nat. Neurosci.*, **9**, 315–321.
42. Kamin, D., Lauterbach, M.A., Westphal, V., Keller, J., Schonle, A., Hell, S.W. and Rizzoli, S.O. (2010) High- and low-mobility stages in the synaptic vesicle cycle. *Biophys. J.*, **99**, 675–684.
43. Staras, K. and Branco, T. (2010) Sharing vesicles between central presynaptic terminals: implications for synaptic function. *Front. Synaptic Neurosci.*, **2**, 20.
44. Fornasiero, E.F., Raimondi, A., Guarnieri, F.C., Orlando, M., Fesce, R., Benfenati, F. and Valtorta, F. (2012) Synapsins contribute to the dynamic spatial organization of synaptic vesicles in an activity-dependent manner. *J. Neurosci.*, **32**, 12214–12227.
45. Orenbuch, A., Shalev, L., Marra, V., Sinai, I., Lavy, Y., Kahn, J., Burden, J.J., Staras, K. and Gitler, D. (2012) Synapsin selectively controls the mobility of resting pool vesicles at hippocampal terminals. *J. Neurosci.*, **32**, 3969–3980.
46. Giannandrea, M., Bianchi, V., Mignogna, M.L., Sirri, A., Carrabino, S., D'Elia, E., Vecellio, M., Russo, S., Cogliati, F., Larizza, L. *et al.* (2010) Mutations in the small GTPase gene RAB39B are responsible for X-linked mental retardation associated with autism, epilepsy, and macrocephaly. *Am. J. Hum. Genet.*, **86**, 185–195.
47. Chin, L.S., Li, L., Ferreira, A., Kosik, K.S. and Greengard, P. (1995) Impairment of axonal development and of synaptogenesis in hippocampal neurons of synapsin I-deficient mice. *Proc. Natl. Acad. Sci. U.S.A*, **92**, 9230–9234.
48. Cancedda, L., Fiumelli, H., Chen, K. and Poo, M.M. (2007) Excitatory GABA action is essential for morphological maturation of cortical neurons in vivo. *J. Neurosci.*, **27**, 5224–5235.
49. Pennuto, M., Dunlap, D., Contestabile, A., Benfenati, F. and Valtorta, F. (2002) Fluorescence resonance energy transfer detection of synaptophysin I and vesicle-associated membrane protein 2 interactions during exocytosis from single live synapses. *Mol. Biol. Cell*, **13**, 2706–2717.
50. Bonanomi, D., Menegon, A., Miccio, A., Ferrari, G., Corradi, A., Kao, H.T., Benfenati, F. and Valtorta, F. (2005) Phosphorylation of synapsin I by cAMP-dependent protein kinase controls synaptic vesicle dynamics in developing neurons. *J. Neurosci.*, **25**, 7299–7308.
51. Amendola, M., Venneri, M.A., Biffi, A., Vigna, E. and Naldini, L. (2005) Coordinate dual-gene transgenesis by lentiviral vectors carrying synthetic bidirectional promoters. *Nat. Biotechnol.*, **23**, 108–116.

52. Czernik, A.J., Girault, J.A., Nairn, A.C., Chen, J., Snyder, G., Kebabian, J. and Greengard, P. (1991) Production of phosphorylation state-specific antibodies. *Methods Enzymol.*, **201**, 264–283.
53. Kalla, S., Stern, M., Basu, J., Varoqueaux, F., Reim, K., Rosenmund, C., Ziv, N.E. and Brose, N. (2006) Molecular dynamics of a presynaptic active zone protein studied in Munc13-1-enhanced yellow fluorescent protein knock-in mutant mice. *J. Neurosci.*, **26**, 13054–13066.
54. Papiani, G., Ruggiano, A., Fossati, M., Raimondi, A., Bertoni, G., Francolini, M., Benfante, R., Navone, F. and Borgese, N. (2012) Restructured endoplasmic reticulum generated by mutant amyotrophic lateral sclerosis-linked VAPB is cleared by the proteasome. *J. Cell Sci.*, **125**, 3601–3611.
55. Hanaichi, T., Sato, T., Iwamoto, T., Malavasi-Yamashiro, J., Hoshino, M. and Mizuno, N. (1986) A stable lead by modification of Sato's method. *J. Electron Microsc. (Tokyo)*, **35**, 304–306.